

Full Length Article

Investigation of the process parameters and restitution coefficient of ductile materials during cold gas dynamic spray (CGDS) using finite element analysis



Sunday Temitope Oyinbo, Tien-Chien Jen*

Department of Mechanical Engineering Science, University of Johannesburg, Gauteng, 2006, South Africa

ARTICLE INFO

Keywords:
 CGDS deposition
 FE simulation
 Process parameters
 Restitution coefficient
 Material jetting

ABSTRACT

Cold gas dynamic spray is a cold spray technique for obtaining solid-state surface coating. Several materials such as metal, metal alloys, composite materials, and polymer have been deposited successfully through cold spray onto a substrate material. A number of industrial applications for cold spray have been developed worldwide in the field of aerospace, energy, automobile, biotechnology, and military applications. In the current study, effects of various processing parameter such as impact velocity, substrate preheating temperature, a combination of different materials and coefficient of friction were used to describe the impact behaviour of ductile materials (copper, Cu, and aluminium, Al) after deposition to find a way of addressing high-strain-rate dynamic problems. The parameters were also used to verify the deposition process for the modelling of cold gas dynamic spray (CGDS) by the Lagrangian approach of finite element analysis. The results of the analysis (simulation) and that of the published experimental results in the literature correlated well. The understanding of the impact behaviour using different parameters was evident by the analysis of temperature and equivalent plastic strain (PEEQ). It was discovered that the deposition process and deformation are largely affected by particle material as compared to the substrate. A lower restitution coefficient was obtained when different materials of varying properties were combined compared to the combination of the same material. Also, the parameters under investigation do not affect the CGDS process individually, as their effects are interrelated.

1. Introduction

Cold gas dynamic spray (CGDS) is a cold spray technique for obtaining solid-state surface coating for fast-growing scientific and industrial applications in the aerospace- repair of solid rocket boosters space shuttle, aircraft industry, gas turbine, petrochemicals, electronics, bioengineering, casting, oil and gas, and automotive industry [1] over the past years. The processing and the deposition resulting from cold gas spraying processes with a wide range of materials have the following advantages: corrosion protection, increase in mechanical durability and wear resistance. It also creates components with different thermal and electrical conductivities than would be yielded by substrate or producing coatings on the substrate components as thermal insulators, high fatigue strength coating, prohibiting creep in an environment with high temperature, clearance control, restoration and repair, prostheses with improved wear, and produce components with attractive appearance [2–4].

CGDS is one of the embracing powder deposition spray processes.

This technology was introduced in Russia by the Institute for Theoretical and Applied Mechanics in the 1980s [5]. Through experimentation, they discovered cold gas spray processes as ‘additive manufacturing’ techniques. Before this time, on August 12, 1902, Thurston patented a method for gas under high pressure at a velocity of 300 m/s to accelerate metallic powder and subsequently, the deposit was achieved by a high-speed collision on the base material. Major innovative development was initiated in the 1950s by Rochevill, using a gas flow at a velocity higher than those obtained with the methods that were commonly used at that time. The flow of gas through a nozzle known as a De Laval Nozzle produced a uniform thin coating [5–7].

Several materials such as metals, metal alloys, composite materials, and polymers were successfully deposited on-to a substrate material by the Russians. Thereby, the high coating deposition rate was attained by the cold gas process. The number of industrial applications for cold spray has increased worldwide in the field of aerospace, energy, automobile, biotechnology, and military. CGDS is a cold spray technique for obtaining solid-state surface coating. The deposition that occurs during

* Corresponding author.

E-mail addresses: soyinbo@uj.ac.za (S.T. Oyinbo), tjen@uj.ac.za (T.-C. Jen).

CGDS can be summarised into the molecular attraction between the surface deposit of the particles and the substrates and in-build deposit growth [62]. A high-speed ranging from 500 to 1500 ms⁻¹ [8] accelerates finely distributed powder particles (ranging from 1 to 50 µm) in a De Laval Nozzle. At supersonic velocity, particles impact and plastically deform on the substrate. The deformation process results in adhesion to the surface [9–15].

Several types of research as mentioned in the literature have been carried out to describe the bonding mechanism and increase the understanding of this phenomenon in the past years [14,16–20,62]. Currently, adiabatic shear instability that occurs at the interfacial zone can be viewed as a widely accepted bonding mechanism as it results from exhaustive localized deformation and high strain rate during the process of deposition. Thermal softening is more dominant in the area where adiabatic shear instability occurs due to adiabatic heating-induction at the interface. This makes it easy at the interface for metals to be extruded because of its viscous nature, which forms outwardly at the rim metal jet [14,21]. On the particle surface, a crack native oxide film exists that can be removed by the help of such a viscous-like metal jet. Hence, metal bonding occurs at the interfacial zone when metal-to-metal contact is initiated [22].

1.1. Numerical approach to cold gas dynamic spray (CGDS) process

The experiment has proven that cold spray deposition processes are difficult to analyse because of their particles and substrate contents [23,24]. Their non-linear nature is responsible for this. Since they have a complex nature that has defied structural and analytical experimentation, the only solution is to introduce computational simulations as a mechanism to study the interactions between particle and substrate for elucidating the bonding mechanism accompanying cold gas dynamic spray.

1.2. CGDS computation simulation

To study the impact behaviour of particle adhesion onto the substrate, numerical simulation using ABAQUS/Explicit was used to predict the deformation process. The use of double impact 3D models with various considerations in the choice of contact interaction, adaptive meshing, element type, and other areas was performed [25,26]. Since at the contact surfaces large deformation always occurs, adaptive meshing was introduced at the beginning of the simulation as a means of coping with the deformation. This was carried out with the sole objective of the preservation of the initial meshing. The ABAQUS/Explicit advection methods were also combined with the mesh grading so as to achieve the desired result. At every 50 increments, the remeshing frequency was kept low in most cases. Adiabatic shear instability causes bonding of particles at the particle and substrate interface as observed by the modelling results at high velocities. It was also observed that the development of non-uniform temperature and strain at the interfacial zone resulted from the confinement of the surface fraction of the bonding.

Li et al. [27] carried out an investigation on oxygen-free high thermal conductivity (OFHC) copper using cold spray particle deformation with the Lagrangian formulation in ABAQUS/Explicit software. To cater for the axisymmetric features that were noticed in their observation, they took the substrate to be a cylinder while using a 2-dimensional symmetrical model. In this model, the particle diameter (d_p) was taken to be one-fifth of the height and radius of the substrate. The contact formulation between particle and substrate used was Explicit (surface-to-surface contact). Other considerations in their analysis are solution procedure, meshing size, interfacial friction, adaptive meshing, element distortion control, hourglass control, and material damage. This numerical analysis was performed in order to investigate the effect of process parameters on the particle impact behaviour, the capacity and feasibility of finite element method (FEM) to analyse the

process by using the ABAQUS/Explicit program. With the correct input parameters and settings, this is a viable method for yielding a satisfactory output. Several other investigations were carried out and published by different authors, which provides more modelling detail techniques on the cold gas dynamic spray deposition process [28–32].

A study was carried out to study the impact behaviour of particles and substrate using another ABAQUS/Explicit model (known as Eulerian Formulation) with Cu as the particle material [33]. It was discovered that a jet was formed at a minimum velocity of about 290 m/s and a maximally attained equivalent plastic strain (PEEQ) was found. This, therefore means that no jet could be formed at a velocity below 290 m/s. This speed was thought to be a critical velocity. At a velocity higher than the range of 290–400 m/s, jet formation discontinued and splashing of material occurred. Therefore, a critical velocity could be predicted through the Eulerian model, as compared to the jet morphology theoretical analysis as a prediction method [34].

By using the following 3D reference frames: Langrangian reference frame (material failure); Arbitrary Lagrangian-Eulerian (ALE) reference frame; Lagrangian reference frame, impact on the semi-infinite substrate by single Cu particles was systematically studied by Yildirim et al. at 100–700 m/s velocities [35]. To demonstrate the process of numerical simulation involving ALE and Lagrangian methods, a 2D axisymmetric model was used, and in furthering this process material failure and Lagrangian simulation approach was carried out using a one-quarter symmetry 3D model. Prior to the initial impact, the particle and substrate were both at 293 K (which was the room temperature). A friction coefficient of 0.3 was used in all cases at a particle substrate interface. The contact formulation used was the penalty and surface-to-surface interaction for axisymmetric 2D simulation. For the 3D simulation of material failure and the Lagrangian model, the use of a general contact algorithm was preferred. Under high deformations, material impact behaviour could be described best using material failure with the Lagrangian approach according to the results of the analysis performed. Furthermore, mesh size was discovered to be responsible for the maximum plastic strain and maximum temperature at the interfacial output. There was a decrease in the plastic strain as interpolation errors occurred when ALE adaptive remeshing techniques were used.

In order to calculate critical velocity during the deposition process, the 3D numerical model was created [36]. The interaction model used in the investigation is general contact without friction at the particle and substrate interface. However, the particle and substrate predictive deformation correlates with the real process. Sobolev space and wavelet transformation were applied by using the second derivative of the physical parameters to solve the problem associated with determining critical velocity as compared to the numerical simulation output observation.

Bae et al. [37] categorized particle and substrate materials according to the metallurgical and physical properties of those materials into four different impact cases namely hard-hard, soft-soft, hard-soft and soft-hard. They use ABAQUS/Explicit software with CAX4R ‘four-node bilinear axisymmetric quadrilateral element mesh’ hourglass control and reduced integration for their simulation from element library. The contact algorithm of the surface to surface particle/substrate interface was used with contact pair formulation. Numerical analysis was performed to study the impact behaviour of 25 µm particle size for all the cases under consideration and characterization was performed by thermos-mechanical modeling. Theoretical and numerical analysis of the thermal boost-up zone (TBZ) was suggested as a result of their analysis. At critical velocities, the TBZ result is inversely proportional to the plastic dissipation energy and the recoverable strain-energy for soft-soft and hard-hard cases. At the soft impact interfacial zone, there is adiabatic shear instability for soft-hard and hard-soft cases. This, of course, is expected as a result of the opposite reaction.

A series of articles have been published focusing on the Smoothed Particle Hydrodynamics (SPH) model, which is another simulation model of cold spray particle deposition process [34,35]. In their

investigations, the Karmel estimate was obtained by using the interpolation of Karmel functions (cubic B-spline) in SPH. First and foremost at the bonding interfacial zone, they made some assumptions that the secondary inter-molecular force is responsible for the bonding strength between the contacting surfaces when the adhesion model was introduced between them. The cohesive zone model introduced by Dugdale-Barenblatt drives the interfacial reaction model by inter-surface traction model, and from the two bodies in contact, the interaction was limited to SPH particles. Meanwhile, the surface contact formation between the two surfaces was mutually confirmed by the activation of this adhesion model. The result generated from this SPH numerical simulation when compared to that of the Eulerian approach yielded similar results in modelling the particle behaviour in cold spraying. This is an indication that particle and substrate impact behaviour can be feasibly simulated by SPH. Particle and substrate interaction could be described by using the cohesive zone model [40].

SPH was used to examine Cu particles impact behaviour using various geometrical impacts of the single, oblique and multiple in cold dynamic spray compared to the Eulerian, Adaptive meshing and Lagrangian approaches [41,42]. According to their investigation, the element type and meshing size greatly affect the output result. Moreover, there is a correlation between the experimental result and the Eulerian formulation than the Langrangian formulation. The Eulerian approach also provides a better result than that of the Lagrangian approach when further study was performed on the multi-particle impact process. Furthermore, SPH numerical approach reveals that the impact behaviour of the particle during deformation relatively yields better output since limited effects of SPH particles independent weight was achieved on the output result.

Another modern numerical method and complex finite element models were used to induce damage in aeronautical structures by Smoijver et al. [43] so as to predict induced damage of bird strike. However, the impacts experienced by the soft body were solved by using the finite element technique called Coupled Eulerian-Lagrangian (CEL) approach. Pressure-density ratio and material volumetric strength by materials equation of state (EOS) were used to model the bird replacement material hydrodynamic response. Experimental results and the Lagrangian bird model were used to validate the result obtained from the bird model using the CEL approach.

CEL bird model exhibits stability in carrying out the analysis due to the fact that significant mesh distortion does not occur in this approach. The higher computational time involved in the CEL approach makes it more disadvantageous to the Lagrangian bird model because, in the CEL approach, more time is required to obtain Eulerian elements fine mesh to accurately carry out simulation of contact between the Eulerian elements and the Lagrangian mesh.

On solving the geotechnical problems, Qiu et al. [44] investigated the capability of the CEL numerical approach. Their result revealed that CEL has the capacity to solve complicated problems that are difficult for FEM to solve. Pile installation was simulated by CEL approach to further examine its capability and it was discovered that CEL is more appropriate to study the installation of pile influence on the relationship between the soil and immediately preceding structure that the values of friction are high if the summation by simulation results and measurements data is anything to go by. In addition, their conclusion is that the CEL approach gives a satisfactory result due to the quality of the parallelization.

Another challenging situation of CGDS process is the nozzle's design which has a great influence on the deposition process. A new simulation model was developed by creating a unified mathematical model to study various processing parameter. They used MATLAB to plot the nozzle contour in 2D form and later simulated the gas flow using computational fluid dynamics (CFD) software i.e. ANSYS Fluent. Their result correlates with the date found in the literature [45,46]. Commercial software FLUENT (Ver 6.1) was used to numerically model the flow field of propellant gas [47,48]. It was discovered that optimized

expansion ratio of nozzle exit diameter is greatly influenced by throat diameter, nozzle divergent cross-sectional length, particles' length and gas conditions. As the nozzle length and gas pressure increase, the optimal expansion ratio increases. It decreases with an increase in nozzle throat diameter, particles' size and gas temperature. When using Helium as the propellant gas, the expansion ratio is higher than that of Nitrogen at the same operating conditions. Several articles that show a modelling technique details published in the literature on the deposition of process by simulation are revealed [45].

1.3. Research objective

To analyse the impact behaviour of a particle on the substrate, several codes of commercial finite element method (FEM) can be utilized, such as ANSYS/LS-DYNA, CHT code and ABAQUS/Explicit. In the coating process, the deposition efficiency can be influenced by some factors such as material combinations and its properties, particle initial impact velocity, frictional coefficient and substrate preheating temperature among others. The experiment has proven that cold spray deposition processes are difficult to analyse because of their non-linear nature [23,24]. Since they have a complex nature that has defied structural and analytical experimentation, the only solution is to introduce computational simulations as a mechanism to study the interactions between particle and substrate for elucidating the bonding mechanism accompanying cold gas dynamic spray. Hence, this study presents multiple particles and substrate impact using ductile materials (copper, Cu and aluminium, Al) to simulate and analyze contact/impact problem of cold gas dynamic spray deposition process and restitution coefficient analysis at the interfacial zone. This was done in order to accomplish a qualitative understanding of cold gas dynamic spray deposition mechanism and find a way of addressing high-strain-rate dynamic problems of cold sprayed particles and substrate. Lagrangian approach in ABAQUS/Explicit was used at controlled contact angle (10^0 - 90^0), impact velocity (300 – 600 m/s), substrate preheating temperature (200–600°C), friction coefficient (0.2–0.5) and four different combinations of materials namely: Copper/Copper, Copper/Aluminium, Aluminium/Copper and Aluminium/Aluminium.

2. Solid model description

ABAQUS/Explicit version 6.14-1, an explicit finite element analysis program, was used to investigate the effects of processing parameters and impact behaviour of ductile materials such as Copper (Cu) and Aluminum (Al) using the Lagrangian approach available in Version 6.14-1. A 3D model was established for the analysis.

In Fig. 1, the Lagrangian domain with particles and substrate assembly is presented with basic dimensions (Fig. (1a)). The height and radius are denoted by the letters H and R while particle and substrate are differentiated by the subscripts p and s respectively. The spherical morphology of the copper particles was used for the numerical model because of the SEM observation (Fig. (1b)). For proper observation, the temperature and plastic strain evolution were studied through two paths, namely the x-direction path and y-direction path. For the Lagrangian numerical analysis approach used in this study, C3D8RT: an 8-node thermally coupled brick, trilinear displacement, and temperature, hourglass control, reduced integration were used for the domain [49]. 0.0003 mm was used as the mesh size i.e., 1/66 D_p resolution. Hexahedral elements were used to carry out the meshing. The penalty formulation, general contact (explicit) was implemented as contact processes available in ABAQUS/Explicit FEA program.

2.1. Material

The description of thermal response is conducted by using the properties of thermal conductivity and specific heat. The properties of the material used in this simulation are entered into the software.

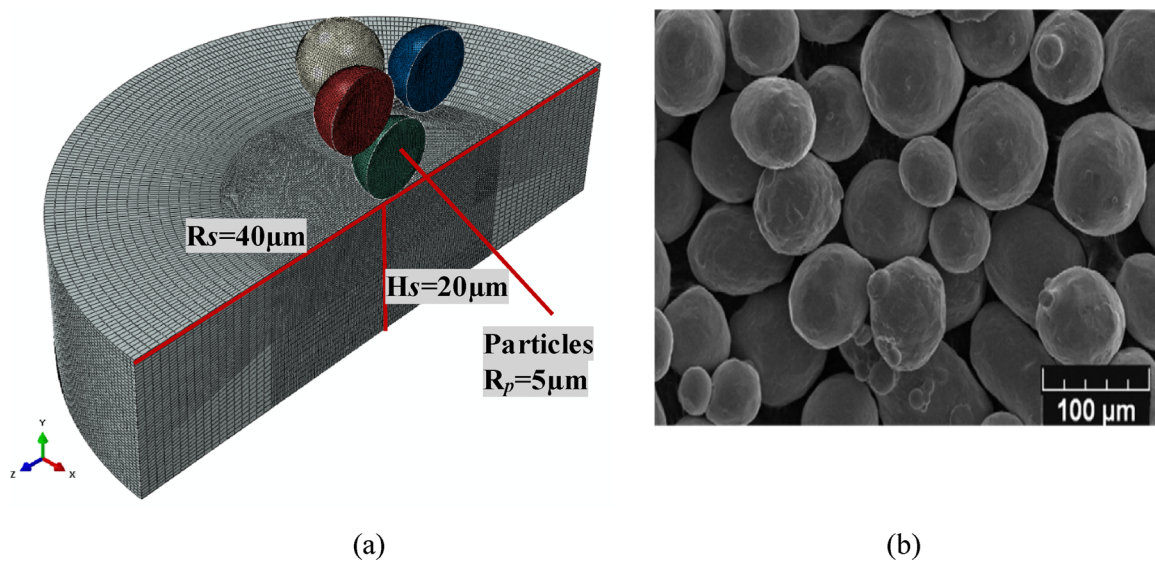


Fig. 1. Schematic diagram illustrating (a) 3-D Lagrangian model (b) Cu particles SEM morphology.

Table 1
Copper and Aluminum material properties used in the numerical analysis [35,37,50].

Properties, Unit, Symbol	Copper	Aluminum
Density, (kg m^{-3}), σ	8.9×10^{-3}	2.7×10^{-3}
Shear modulus, (GPa), G	44.7	27
Thermal conductivity, (W/m.K), λ	386.5	237.2
Specific heat, (J/kg.K), c	383	898.2
Sound velocity, (m/s), C_0	3940	5386
U_s versus U_p , (-), s	1.489	1.339
Grüneisen coefficient, (-), Γ_0	2.02	1.97
Yield stress, (MPa), A	90	148.4
Hardening constant, (MPa), B	292	345.5
Hardening exponent, (-), n	0.310	0.183
Strain rate constant, (-), C	0.0250	0.001
Thermal softening, (-), m	1.090	0.895
Melting temperature, (K), T_m	1356	916
The reference temperature, (K), T_0	298	293

Table 1 shows the materials used in the simulations and their properties at room temperature [35,37,50]. The material elastic response is on the assumption of the Mie-Grüneisen Equation of State (EOS), in which the linear elasticity model was used.

In ABAQUS/Explicit program [49], the internal energy per unit mass (E) and the density (ρ) are used to determine the pressure P as illustrated in Eqs. (1)–(7). Here E_m , c_0 , S , Γ_0 , ρ , and ρ_0 are the internal energy with reference to a specific volume, sound bulk speed, linear Hugoniot slope coefficient, the material constant known as Grüneisen's gamma, current density and initial density respectively. Also, the nominal volumetric compressive strain is indicated by the following:

$$\eta = 1 - \frac{\rho}{\rho_0}$$

$$P - P_H = \Gamma \rho (E_m - E_H) \quad (1)$$

The Hugoniot specific energy (E_H) and pressure (P_H) are only the density functions, and the Grüneisen ratio is outlined as:

$$\Gamma = \Gamma_0 \frac{\rho_0}{\rho} \quad (2)$$

The reference density is the Γ_0 and ρ_0 . The relationship between the Hugoniot specific energy (E_H) and Hugoniot pressure are given as:

$$E_H = \frac{P_H \eta}{2\rho_0} \quad (3)$$

The nominal volumetric compressive strain is indicated by the

following: $\eta = 1 - \frac{\rho}{\rho_0}$. The above equation yields Eq. (4) by eliminating Γ and E_H .

$$P = P_H \left(1 - \frac{\Gamma_0}{2} \right) + \Gamma_0 \rho_0 E_m \quad (4)$$

The energy equation and equation of state are used as coupled equations for internal energy and pressure. These equations are solved simultaneously by ABAQUS/Explicit at each material point. Hence, Hugoniot data yields:

$$P_H = \frac{\rho_0 c_0^2 \eta}{(1 - s\eta)^2} \quad (5)$$

Where U_s , the linear shock velocity and U_p , the particle velocity is defined by the linear relationship between c_0 and s as follows:

$$U_s = c_0 + sU_p \quad (6)$$

Hugoniot form (U_s - U_p) can be linearly expressed follow the above assumptions as follow:

$$P = \frac{\rho_0 c_0^2 \eta}{(1 - s\eta)^2} \left(1 - \frac{\Gamma_0 \eta}{2} \right) + \Gamma_0 \rho_0 E_m \quad (7)$$

Where $\rho_0 c_0^2$ is equivalent to the elastic bulk modulus at small nominal strains.

The description of material flow for both the particle and the substrate is given by the Johnson-Cook plasticity model [28]. The Strain rate hardening, the strain hardening, and temperature softening are the three basic functions of flow stress, σ as illustrated in Eq. (8) where the equivalent plastic strain denoted by $\dot{\epsilon}$, working hardening exponent n, $\dot{\epsilon}_0 = 1.0 \text{ s}^{-1}$, the dimensionless plastic strain rate is the ratio of $\dot{\epsilon}/\dot{\epsilon}_0$ and material constants A, B, C, and m have their values given in **Table 1**. T , T_m , and T_0 are the measured temperature, melting temperature and reference temperature respectively.

$$\sigma = (A + B\dot{\epsilon}^n) \left[1 + C \ln \left(1 + \frac{\dot{\epsilon}}{\dot{\epsilon}_0} \right) \right] \left(1 - \left[\frac{T - T_0}{T_m - T_0} \right]^m \right) \quad (8)$$

2.2. Parametric outline of the simulation

To better understand the formation of a coating mechanism, the particle/substrate impact must be investigated for a greater understanding of the phenomenon. This work presents the interaction between four particles with the surface of the substrate. The deformation

Table 2

Schematic calculation plan used in the simulation to study the effects of parameters.

CASE Parameter	CASE 1 Velocity	CASE 2 Temperature	CASE 3 Coefficient of Friction	CASE 4 Material
Size (μm)	20	20	20	20
Material	Copper/Copper	Copper/Copper	Copper/Copper	Copper/Copper, Copper/Aluminum, Aluminum/Copper, Aluminum/Aluminum
Velocity (ms^{-1})	300,400,500,600	500	500	500
Temperature (K)	25	25,200,400,600	25	25
Contact angle ($^\circ$)	90	90	90	90
Friction	0.2	0.2	0.2, 0.3, 0.5	0.2

behaviour of particle/substrate during impact is basically dependent on the makeup of the contacting solid bodies i.e. visco-plastic, visco-elastic, work hardening elastic-plastic, elastic-perfectly plastic and elastic solids. This research only considers the isotropic work hardening of elastic-plastic materials impact. **Table 2** shows the parametric study outline, in which attention was given to various processing parameters such as impact velocity, particles initial temperature, combination of different materials and coefficient of friction to describe the impact behaviour of ductile materials after deposition to find a way of dealing with deformation problem of high strain rate using the Lagrangian approach.

2.3. Boundary conditions

The Lagrangian model developed for this work consists of Copper (Cu) particle and Cu substrate. The substrate base was fixed completely. The adiabatic process was assumed for the process of particle and substrate impact according to Assadi et al. [14]. The initial temperature for both the particle and the substrate was assumed to be at room temperature of 25°C for all calculations. Finally, the monitoring of the outputs generated from the simulation was done by Python script code during impact for the element that experienced the maximum equivalent plastic strain (PEEQ).

3. Results and discussion

3.1. The profile of the deformed

The deformation of the materials in the whole process changes from one phase to another when they are in contact as a common phenomenon to engineering materials. The deformation is fully plastic from a region of elastic-plastic. However, in the beginning, it was purely elastic. In thermal sprayed coating, there are usually three stress components: peening stress, thermal stress, and stress-induced by quenching [51]. Here, it is observed that the dominant stress is the peening stress as indicated by the compressive stress. The generation of peening stress during the deposition, in a high-velocity impact cold spray process is because of substrate plastic deformation and/or coating material previously deposited. At an initial velocity of 500 m/s, Cu/Cu impact consists of the deformation section (compression) followed by the rebound section. **Fig. 2** shows the deformation of Cu/Cu after impact from the typical 3D-numerical simulation results with four-particles plastically deformed on the substrate **Fig. 2(c)** and the typical experimental observation (**Fig. 2(a,b,d)**) [52], and after the particle/substrate impact, **Fig. 3** and **Fig. 4** shows the shape evolution at different impact times of 60 ns for equivalent plastic strain (PEEQ) and TEMP respectively. In these figures, one can see that there is a reduction in the particle aspect ratio (height-to-width) with an increase in the contact time collision process, while the width and the depth of the substrate create upsurge.

In addition, at 15 ns impact time (**Fig. 4(a)**), near the contact area region, well-built compressive stress has already been induced and increased by the impact of supersonic velocity and the interfacial temperature accordingly. The temperature (TEMP) and maximum

equivalent plastic strain (PEEQ) region are localised at the interfacial zone edge and not at the centre where the initial impact occurs. A jet is created at the interfacial zone by particle and substrate materials as the particle and substrate deformation continues and the deformed particle now has a lens-like shape. Then, more jet is formed as the particle and substrate materials deform further. **Figs. 3(c)-(f)** and **4(a)-(f)** show the impact time history of the jet evolution for the PEEQ and the Temperature (TEMP) distribution with an impact time history of 60 ns. It can be seen from these figures when compared with the literature [53], the shear change occurrence of PEEQ and TEMP evolution is not sufficient to clearly detect adiabatic shear instability.

Fig. 5 (a)-(f) show the Von Mises Stress evolution at the time interval of 60 ns. For Cu material, the work hardening, and plastic deformation increases the flow stress. As shown in **Fig. 5(a)-(f)**, the stress wave spreads from the interfacial zone to the substrate boundary as the deformation progresses because the induced Von Mises Stress increases. It was an indication from the stress distribution that particle rebound has occurred in **Fig. 5(d)** even though the particles and the substrate are still in contact. The detachment of the particles from the substrate at 40 ns causes the particles to have a small region of tensile stress which occurs locally inside the particles (**Fig. 5(e)**).

At the end of the calculation, a visible boundary was created between the particles and the substrate (**Fig. 6(f)**), and after removing the impact loading, the residual stresses are permanently induced in the particles and the substrate.

3.2. Impact velocity

The focus of many researchers in the literature is often based on the interface or the particle but not on the substrate [22,53,55]. But the substrate is also sensitive to the change in impact velocity. At various times, **Fig. 6** shows the evolutions of temperature (TEMP) and equivalent plastic strain (PEEQ) of the Cu/Cu contact surface in the radial direction over the contact zone. It can be clearly observed that from the centre of the contact region, both the TEMP and the PEEQ increase significantly as the deformation progresses with time along the horizontal direction which implies that the Cu material at the contact region becomes softer and plastically deforms than the Cu substrate material at the other region and thus the particles move relatively with substrate surface. When particle rebounding occurs, the TEMP and PEEQ increase with time after 20 ns.

Fig. 7 shows the evolution of the temperature (TEMP) and the equivalent plastic strain (PEEQ) within the substrate at the time history of 60 ns after impact. It can be noticed that after 5 ns, the PEEQ increases. This is due to the change that occurs at high impact velocities from plasticity to viscous flow in the deformation region. This effect accounts for the thermal softening in this present analysis and is attributed to the third term of strain-stress law in the Johnson-Cook model.

The temperature increases sharply between the period of 5 ns and 40 ns due to the high strain rates ($10^5 - 10^7 \text{s}^{-1}$). Subsequently, the surface of the substrate is slowly cool down. Generally, as the impact velocity increases, equivalent plastic strain, substrate's temperature, and plastic strain rate also increase.

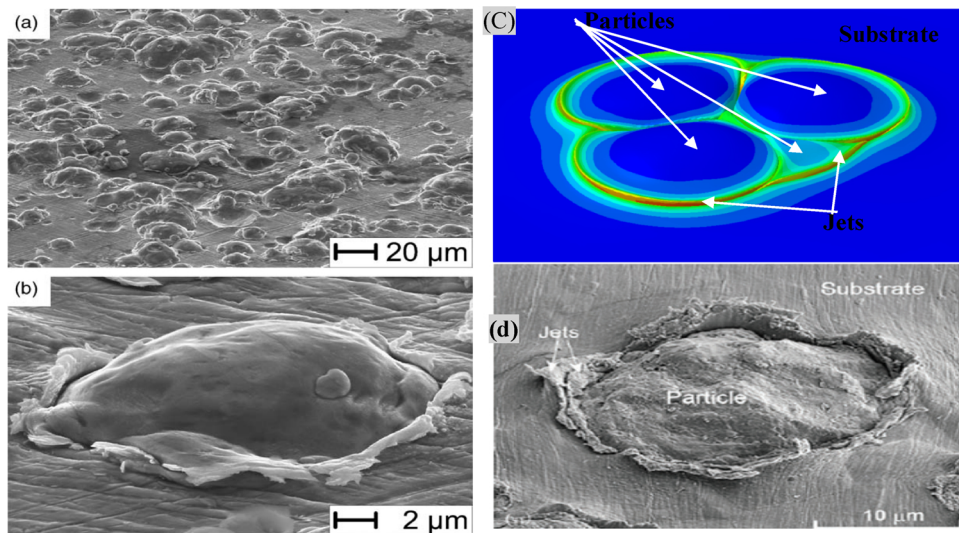


Fig. 2. The deformation of Cu/Cu after impact at an initial velocity of 500 ms^{-1} . (a) SEM Overview (b) SEM close-up image [54] (c) typical 3-D simulation results (d) SEM close-up image [52].

The resultant computed distributions of the substrate's surface TEMP and the PEEQ along the radial direction are shown in Fig. 8 at varying impact velocities. These distributions are clearly seen to be essentially identical. The influence of the impact velocity on the substrate surface is much larger than at the depth of the substrate. Evidently, higher impact velocities during impact generate greater maximum PEEQ and higher maximum TEMP. The contact area increases with increasing impact velocity because the value of the maximum resultant area spreads to the right. Quantitatively, the maximum temperature and the maximum equivalent plastic strain increase respectively, 36.7 % and 12.83 %, when the impact velocity increases from 300 m/s to 600 m/s.

3.3. Substrate pre-heating temperature

Fig. 9 shows the effect of different pre-heating temperatures at the impact time history of 60 ns of 500 m/s on the PEEQ and the TEMP in the Cu substrate when multiple Cu particles are deposited. It can be observed in each case that a deep crater is formed by the Cu particles cold sprayed on the surface of the substrate at high-velocity impact. At the interfacial zone, plastic deformation locally occurs as plastic work dissipation in this region increases the adiabatic temperature in the region. At the increase of preheating temperature, the deformation experienced by the substrate increases.

Thermal softening enhances the level of deformation in the pre-heated substrate by enabling the material to deform easily and eliminate the effect of work hardening (Fig. 9(a)). Thermal softening is responsible for the increase in the plastic strain after 2 ns of contact

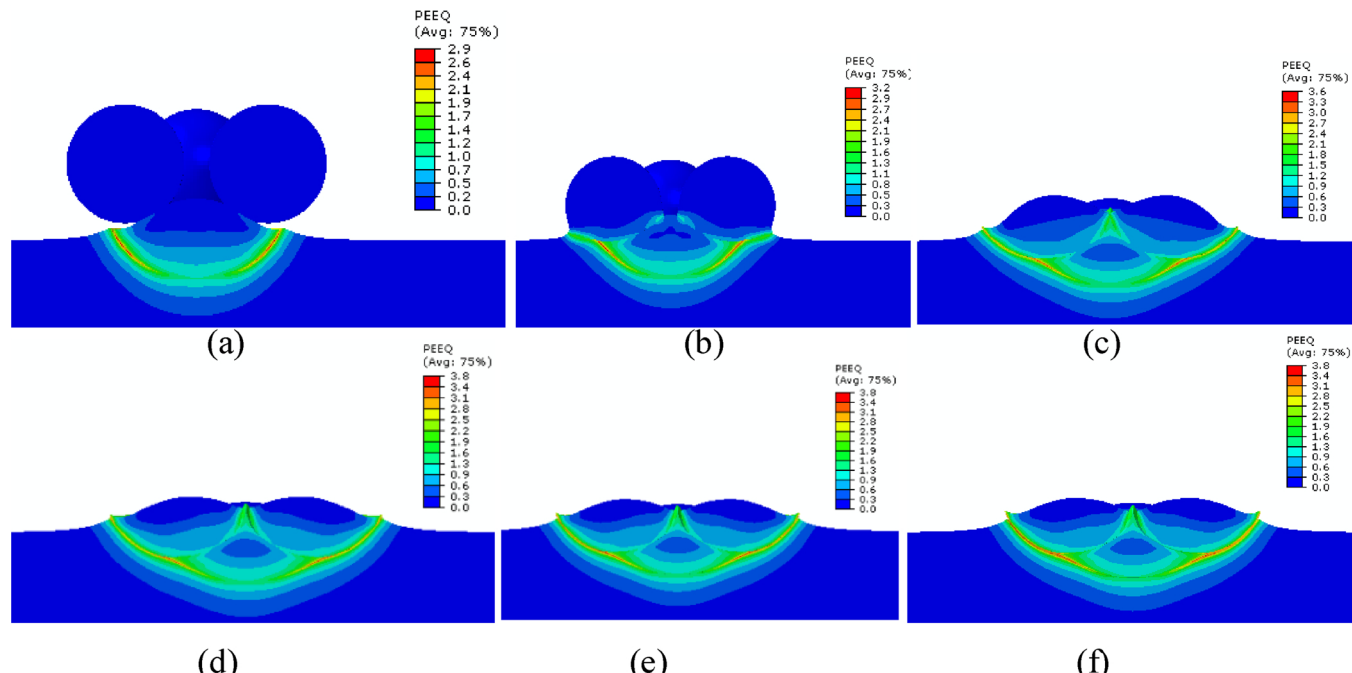


Fig. 3. The Equivalent plastic strain evolution (PEEQ) at 500 ms^{-1} Cu/Cu impact at different impacting times of (a) 15 ns (b) 20 ns (c) 30 ns (d) 40 ns (e) 50 ns (f) 60 ns.

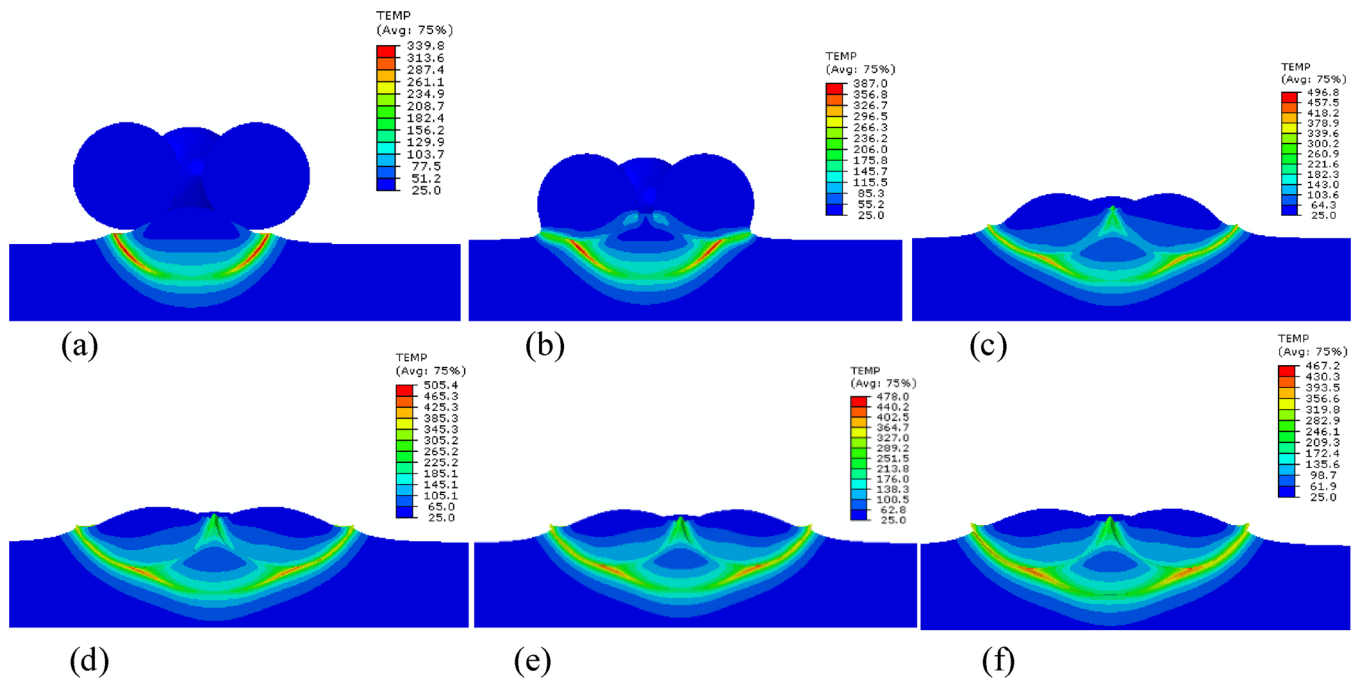


Fig. 4. The TEMP at 500 ms^{-1} Cu/Cu impact at different impacting times of (a) 15 ns (b) 20 ns (c) 30 ns (d) 40 ns (e) 50 ns (f) 60 ns.

time (Fig. 9(b)). As the melting temperature of the material approaches, the shear flow material resistance is generally small due to the thermal softening effect. This is the reason that a lower TEMP ratio and higher PEEQ are attained at higher pre-heating temperature (Fig. 10). Therefore, as the substrate pre-heating temperature increases the material jet formed at the edge of the interfacial region is more and more noticeable. The crater depth created within the substrate shows that as the pre-heating temperature increases, the crater depth also increases (Fig. 11 (a)-(d)).

The temperature of heated gas in the commercial cold spray process

is up to 527°C - 827°C depending on the technology used. The investigation carried out by some researchers revealed that high impact energy like the one experienced during explosion welding gives rise to local particle melting at the interfacial region during particle and substrate impact [19,38]. On the contrary, these premises have been rejected by other authors on the bases that adhesion at the interface is solely by extremely localized pressure which generates local plastic deformation in this region [39,41].

Fig. 11 (a)-(d) also illustrates the temperature distribution of the impact for pre-heating temperature varying from 25°C - 600°C . The

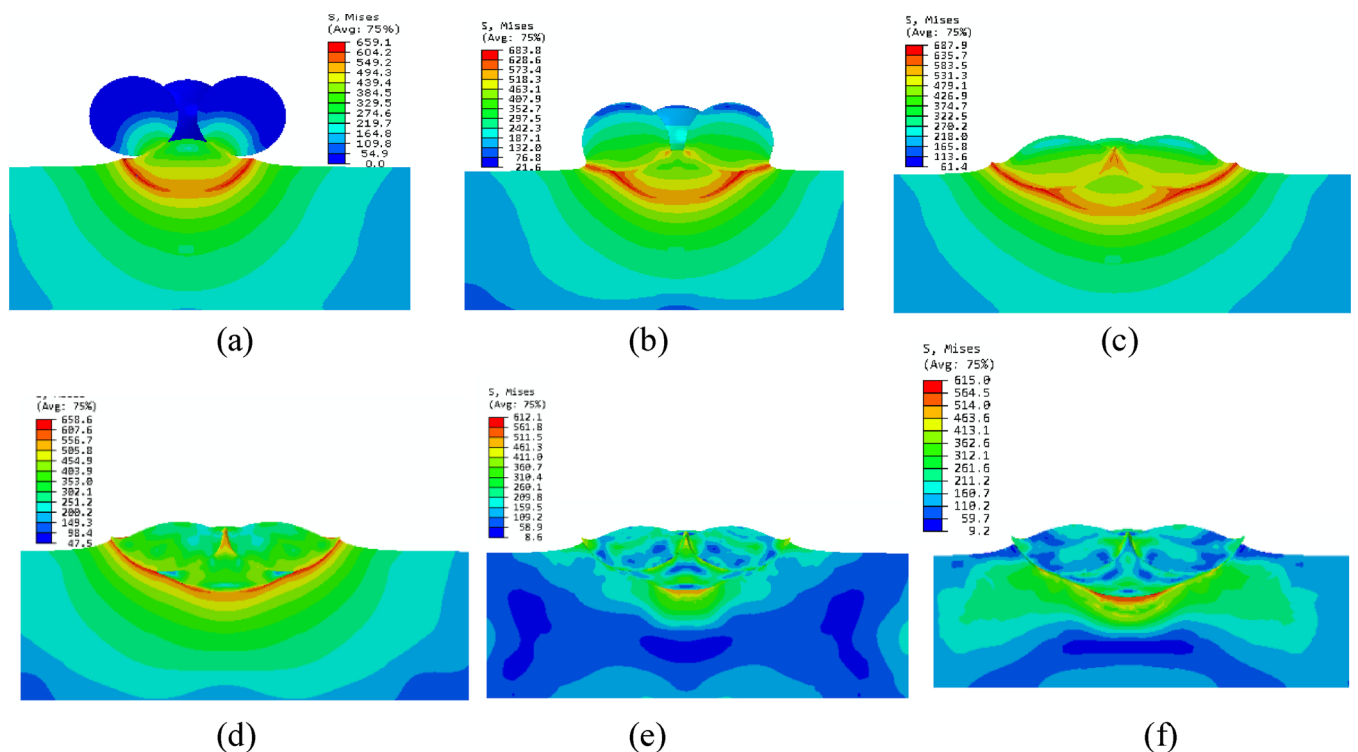


Fig. 5. The mean stress evolution at 500 ms^{-1} Cu/Cu impact at different impacting times (a) 15 ns (b) 20 ns (c) 30 ns (d) 40 ns (e) 50 ns (f) 60 ns.

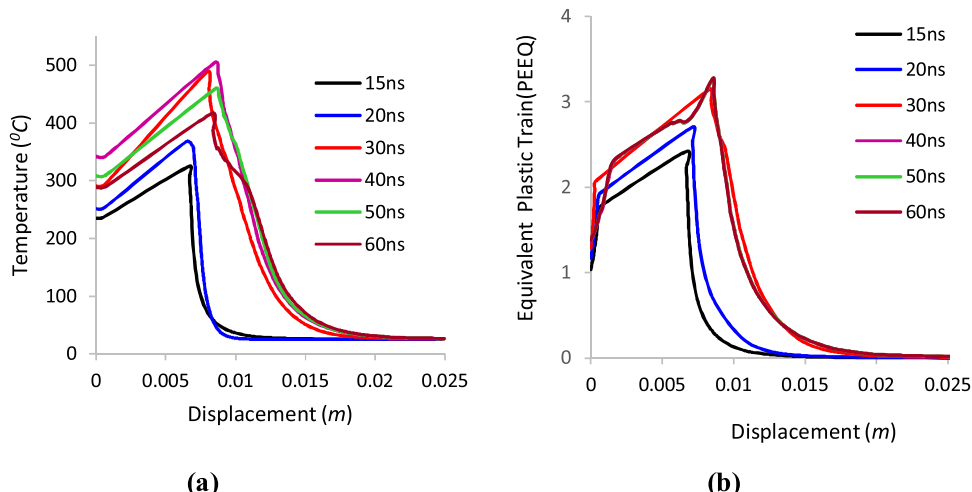


Fig. 6. The distribution at the interfacial zone of (a) TEMP and (b) PEEQ along the radial direction of the Cu/Cu contact surface with the initial impact velocity of 500 ms^{-1} .

maximum temperature attained with 600^0C pre-heating temperature of Cu particles is 996.4^0C . This temperature is below the Cu melting temperature of 1083^0C . There is no melting at the interfacial region when the preheating temperature is 200^0C and 400^0C because the temperature at the interface throughout the process is less than the melting temperature. The interfacial region where the actual impact occurs can experience higher temperatures than the melting temperature of spray materials because of adiabatic shear instability which produces a thin melted coating. But in the case of Cu/Cu, no thin melted layer or localized region is found.

3.4. Friction coefficient

Fig. 12 shows the effect of friction coefficient at the impact time history of 60 ns on the PEEQ and the TEMP in the substrate at the impact velocity of 500 m/s . In the beginning, the increase rate of the TEMP and the PEEQ was rapid between 2 ns and 10 ns, and subsequently, become slow until the calculation was concluded. The ‘two-step behaviour’ displayed in Fig. 12 (a) and (b) is due to the impact of the fourth particle between 10 ns and 25 ns.

As the coefficient of friction increases, the PEEQ increases at the

substrate surface. However, the influence of frictional energy is very little with increasing substrate temperature. The difference is very little between the maximum TEMP and the maximum PEEQ obtained with a 0.2 and 0.5 coefficient of friction. In all cases of the coefficient of friction, the friction energy only constitutes at most 1.2 % of the internal energy, as shown in Fig. 13. The friction influence is not pronounced when the particle/substrate impact is less than 15 ns and its effect on the internal energy is less than 0.24 % but increases thereafter. An increase in the coefficient of friction reduces the friction energy due to the fact that the sliding distance will be shorter and consequently, the distance reduces friction energy. The resultant distribution of PEEQ and TEMP are shown in Fig. 14 for the various coefficient of friction of the surface of the Cu substrate along the radial direction. When the effect of the coefficient of friction is compared to the effect of other parameters outlined in this research, it is relatively small.

3.5. The material combination of different ductile metals

Fig. 15 shows the effect of the combination of different ductile materials (copper, Cu, and aluminium, Al) at the impact time history of 60 ns on the PEEQ and the TEMP in the substrate at an impact velocity

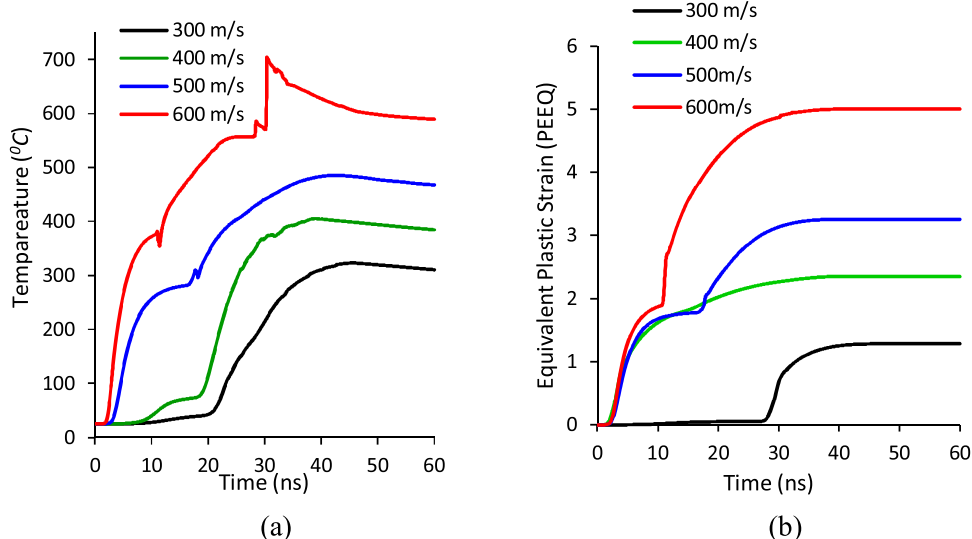


Fig. 7. The evolution of (a) The TEMP (b) The PEEQ of Cu/Cu impact at 300 ms^{-1} , 400 ms^{-1} , 500 ms^{-1} and 600 ms^{-1} impact velocity using the Lagrangian approach.

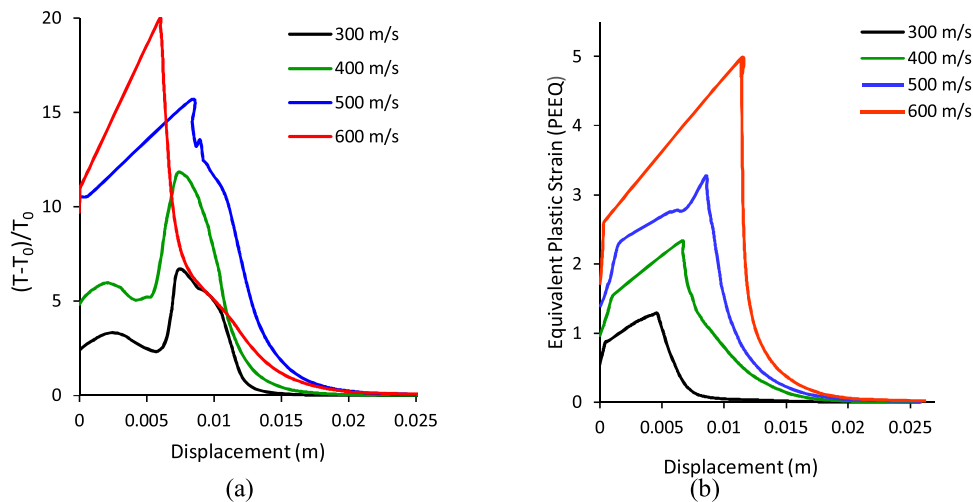


Fig. 8. The resultant computed distributions of (a) The TEMP and (b) the PEEQ along the radial direction at 300 ms^{-1} , 400 ms^{-1} , 500 ms^{-1} and 600 ms^{-1} impact velocity using the Lagrangian approach.

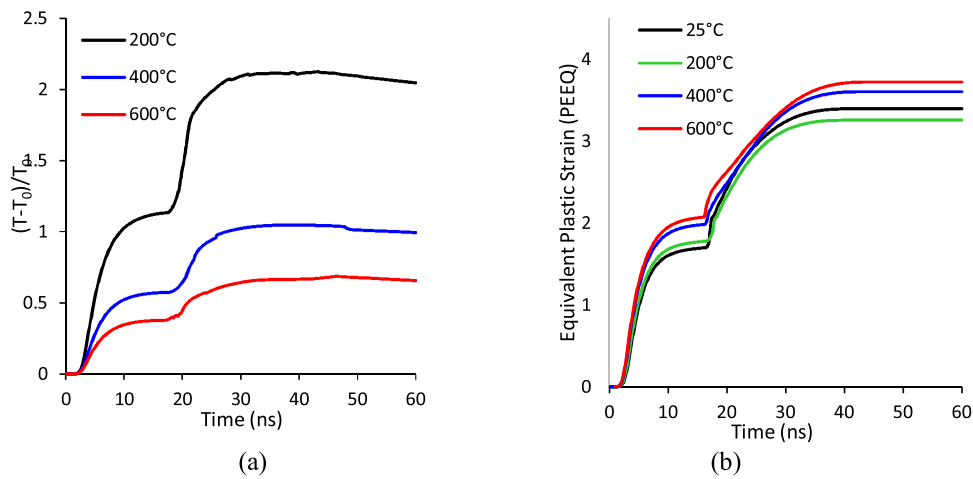


Fig. 9. The impact time of (a) The TEMP (b) PEEQ with pre-heating temperature of 200°C , 400°C and 600°C of Cu/Cu by using the Lagrangian approach at 500 m/s .

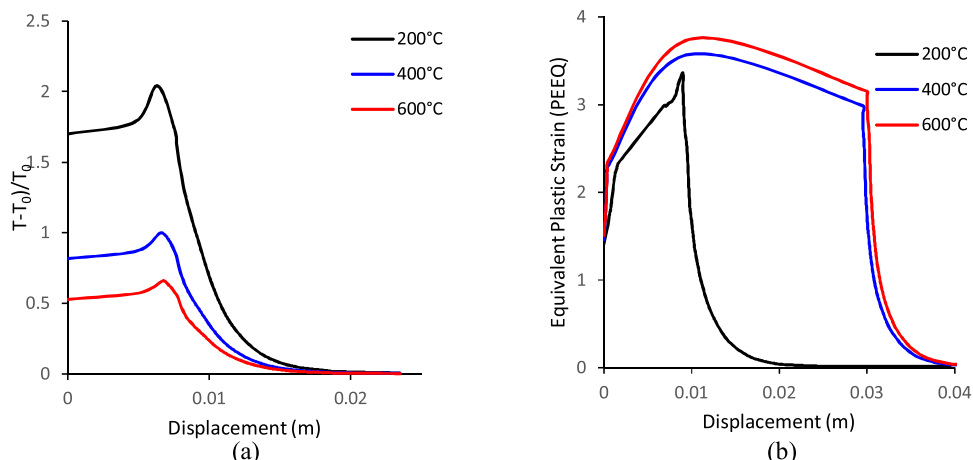


Fig. 10. The distribution of temperature (TEMP) (a) along the horizontal path and (b) impact time histories with pre-heating temperature of 200°C , 400°C and 600°C of Cu/Cu by using the Lagrangian approach at 500 m/s .

of 500 m/s . Since the density of Copper is higher than Aluminium, the initial kinetic energy of copper particles is higher with equal impact velocity and radius and more plastic deformation is significant in the Cu particles (Fig. 15(b)) and higher temperatures are attained (Fig. 15(a)). The particle and substrate and the deposition process are influenced in

a greater way by the particle material than by the substrate material. The deposition process and the deformation are predominantly affected by the particle material, rather than by that of the substrate. The development of PEEQ in all cases of Cu impact (Cu/Al and Cu/Cu) are similar despite the substrate material being different, hence the Al

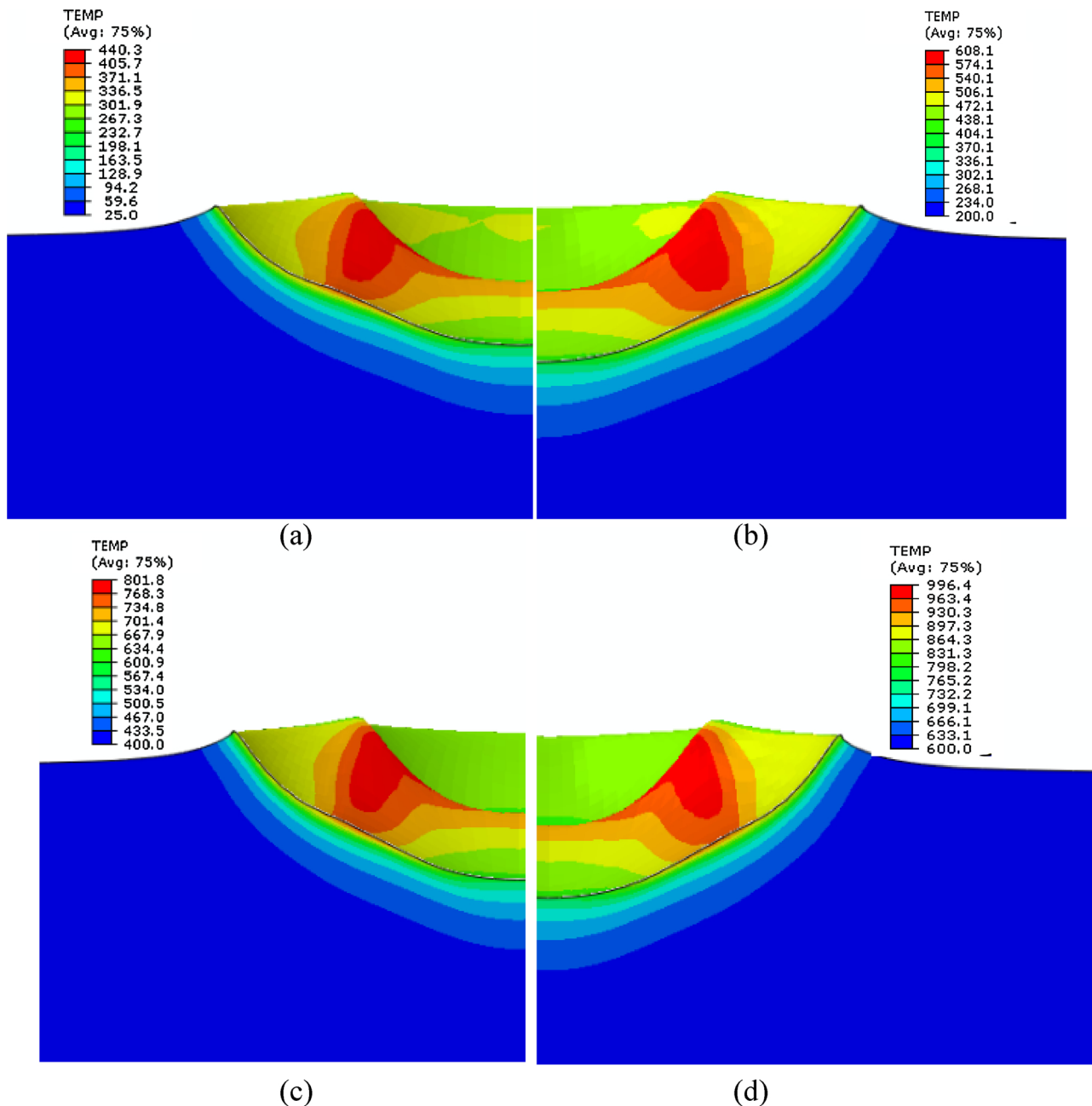


Fig. 11. The evolution of TEMP at 500 ms⁻¹ Cu/Cu impact at different pre-heating temperature of (a) 25°C (b) 200°C (c) 400°C and (d) 600°C showing different crater depth.

impact.

Fig. 16 shows the kinetic energy developed for 60 ns impact time of different materials combined at 500 ms⁻¹. Both the contact time of Al/Cu as well as the plastic deformation are considerably smaller when compared to the other three combinations. Contact time, as indicated in Fig. 16 (a), for Al/Cu is 30 ns, Al/Al is 35 ns, Cu/Al is 40 ns and Cu/Cu is 45. At [21], 634 ms⁻¹ and 766 ms⁻¹ are the approximated critical velocities for Al/Cu and Al/Al respectively. The 500 ms⁻¹ impact velocity selected for this simulation falls below its critical velocity, and the contact time is very short for the rebound of Al particles. 571 ms⁻¹ and 507 ms⁻¹ are the approximate critical velocities for Cu/Cu and Cu/Al respectively [21]. Cu particles deform plastically with enough contact time because the critical velocity is close to the impact velocity. Fig. 16 (b) shows that the kinetic energy developed after the particle has rebounded is not monotone. In fact, the kinetic energy was damped periodically, and if the impact time is longer than the impacts of

the second particle, the particle vibration may eventually stop.

Fig. 17 shows the effect of combinations of different ductile materials at the impact velocity of 500 ms⁻¹ on the calculated PEEQ and the temperature distribution along the radial direction. The contact area projected by Cu/Al and Cu/Cu due to the extended contact impact time and higher kinetic energy of Cu particles is higher than the contact area projected by Al particles. Moreover, the value of PEEQ approaches zero when the substrate depth and the radii are two times and four times the particle radius respectively. It can be noted that a thin surface layer of the substrate is affected by temperature increase. Therefore, the efficiency and accuracy of this model dimension are suitable to study the multiple-impact process.

3.6. Energy dissipation and restitution coefficient

The post-impact motion of the particle can be predicted by the

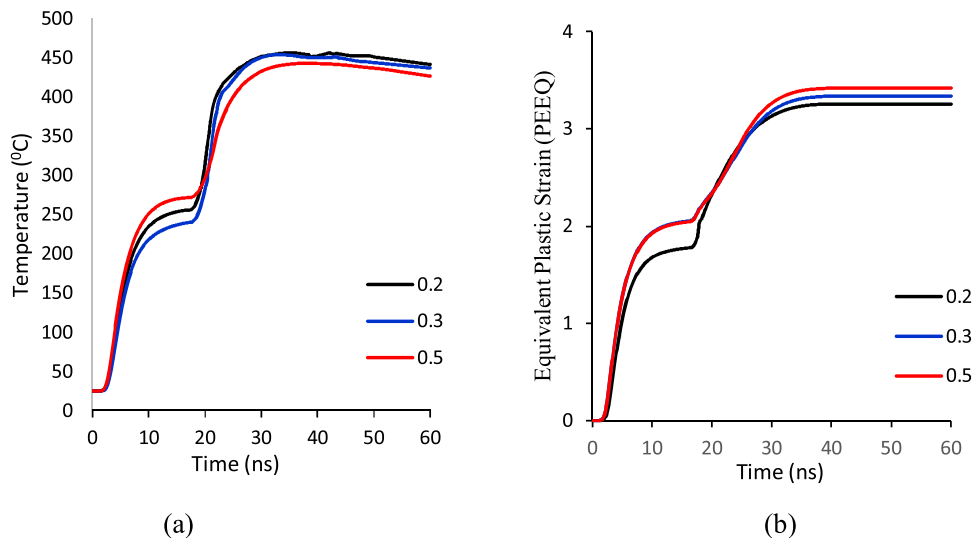


Fig. 12. The impact time of (a) the temperature (TEMP) (b) the equivalent plastic strain (PEEQ) with coefficients of friction 0.2, 0.3, and 0.5 of Cu/Cu by using the Lagrangian approach.

restitution coefficient which is one of the important parameters used during the impact to describe the variation in kinetic energy. STRONG, POISSON and NEWTON [56] proposed several definitions for the restitution coefficient. According to Newton, the restitution coefficient e relates the relative velocities before and after the impact [57] as:

$$V_{1r} - V_{2r} = -e(V_{1i} - V_{2i}) \quad (20)$$

The subscripts i and r represent the initial impact and rebound state respectively while 1 and 2 stand for the particle and substrate respectively.

During the deposition process of Cold Spray, there is a transformation of energy from initial kinetic energy (ALLKE) to the energy stored in the particle and substrate in other word the elastic-stain energy (ALLSE), the energy to plastically deform the material: the plastic strain energy (ALLPD) and the stress wave propagation energy. Once the material has been plastically deformed, the process is irreversible and the energy that can be recuperated during the restitution is the stored kinetic energy. This energy is called the rebound kinetic energy.

Within the particle, Fig. 18 shows the dissipation of initial kinetic energy and how it is transmitted into plastic strain energy in the substrate, thereby producing plastic deformations, of which ALLPD (plastic strain energy) is 91 % of ALLIE (internal energy). The loss of initial kinetic energy only amounts to 9 % due to stress wave propagation. Therefore, rebound velocity can be alternatively calculated from the rebound kinetic energy as follows:

$$V_r = \sqrt{\frac{2E_r}{m}} \quad (21)$$

Where m and E_r represent the mass of the particle and rebound kinetic energy, respectively. Hence, the restitution coefficient is outlined in Eq. (22) where the initial kinetic energy is represented by E_i and E_r represents the rebound kinetic energy. Fig. 19 shows the restitution coefficients for different parameters at 60 ns impact calculation time.

$$e = \sqrt{\frac{E_r}{E_i}} \quad (22)$$

Fig. 19 (d) shows that material is the factor that significantly affects or influences the restitution coefficient.

A similar material combination has a higher restitution coefficient as compared with a dissimilar material combination. The parameter that least affects the restitution coefficient is the coefficient of friction as shown in Fig. 19 (c). As the impact velocity increases, the restitution coefficient also increases slightly, and this may be because of the material strain hardening. It is worth noting that when critical velocity is far above impact velocity, then the increase in impact velocity increases linearly with the restitution coefficient. If the critical velocity is lower than the impact velocity, the restitution coefficient will decrease as the ability for the material to store elastic energy is lost due to the fast rate of deformations, or in some instances damage the material [58,59] (Fig. 19(a)).

The decrease in the restitution coefficient also results from

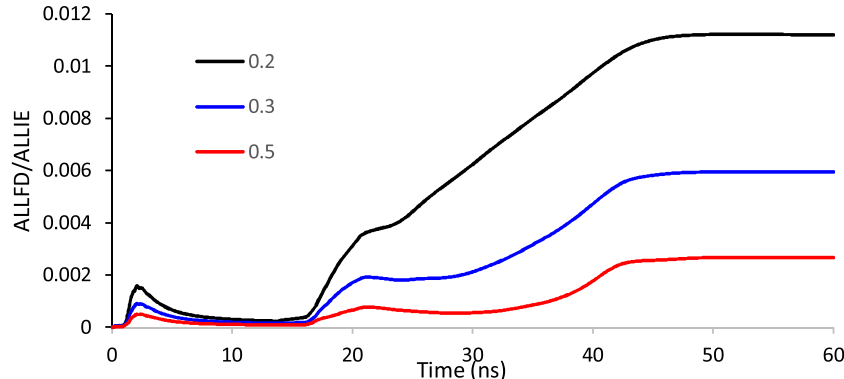


Fig. 13. The impact time histories of the ratio of ALLFD/ALLIE with coefficients of friction 0.2, 0.3, and 0.5 of Cu/Cu impact using the Lagrangian method. ALLFD- Friction Energy; ALLIE- Internal Energy.

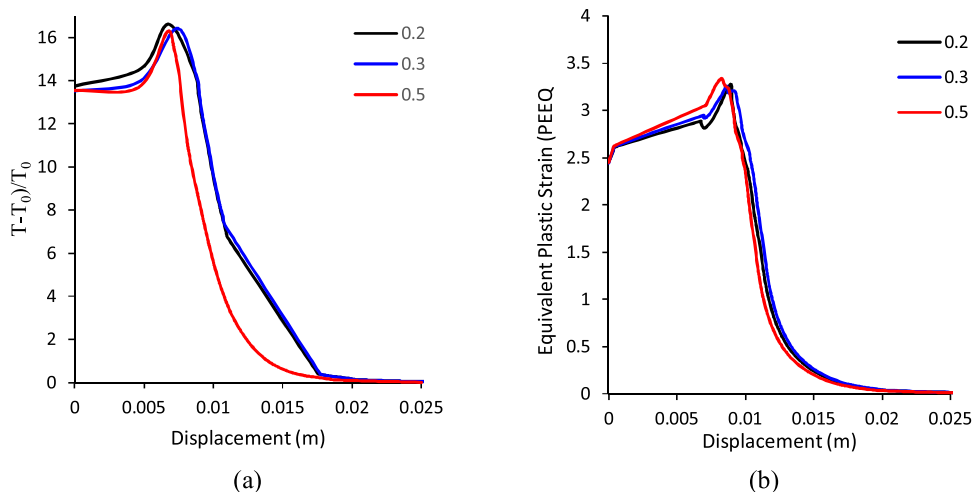


Fig. 14. The distribution of (a) the temperature (TEMP) and (b) the equivalent plastic strain (PEEQ) with coefficients of friction 0.2, 0.3, and 0.5 of Cu/Cu by using the Lagrangian approach.

decreasing the particle initial temperature as shown as Fig. 19 (b). Temperature is a determining factor of the material mechanical property. Therefore, the deformation of a particle requires less kinetic energy. When the particle has a higher initial temperature, extra recoverable strain energy is stored in the process. From this analysis, the zero value of restitution coefficients is not recorded because when the particle impact velocity is significantly higher than the rebound velocity, the value for the restitution coefficient is zero. This implies that at impact, the particle remains at the substrate surface because its motion has stopped, and the particle has bounded with the substrate [38,60].

3.7. Discussion

This study considered four parameters such as impact velocity, substrate preheating temperature, a combination of different materials and coefficient of friction used to describe the impact behaviour of ductile materials such as (copper and aluminium) after deposition.

The deposition process is greatly affected by the choice of materials. It cannot be emphatically stated that the same material combination is better than using different combinations of materials, or when the substrate is hard is better than when it is soft. The material choice is a factor of the machine costs, the service life, the coating application,

and, even ecological effects. The optimisation of the substrate pre-heating temperature and the impact velocity follows the selection of the materials.

In summary, the parametric effects on the output generated in this study are schematically presented in Table 3, including PEEQ and TEMP increments. The temperature increments here are precisely matched to the substrate pre-heating temperature. However, it can be recalled that the particle velocity and the geometry of the nozzle in the cold spray process depend largely on each other as well as on the pressure of the gas that flows through the nozzle. Particle and substrate metallic bonding are greatly favoured at higher interfacial temperature.

Consequently, if any of these process parameters (temperature or pressure of the carrier gas, nozzle geometry) changes, it affects both the particle velocity and the temperature of the substrate.

In addition, if the substrate is preheated prior to impact, it is expected that the value of the critical velocity (velocity below which particle rebound occurs) will be lower. This agrees with Lee et al. [61] experimental results, which state that at 100 K increase of propellant gas temperature, the critical velocity decreases by 50 ms^{-1} . A lower restitution coefficient was obtained when different materials of varying properties are combined compared to the combination of the same material.

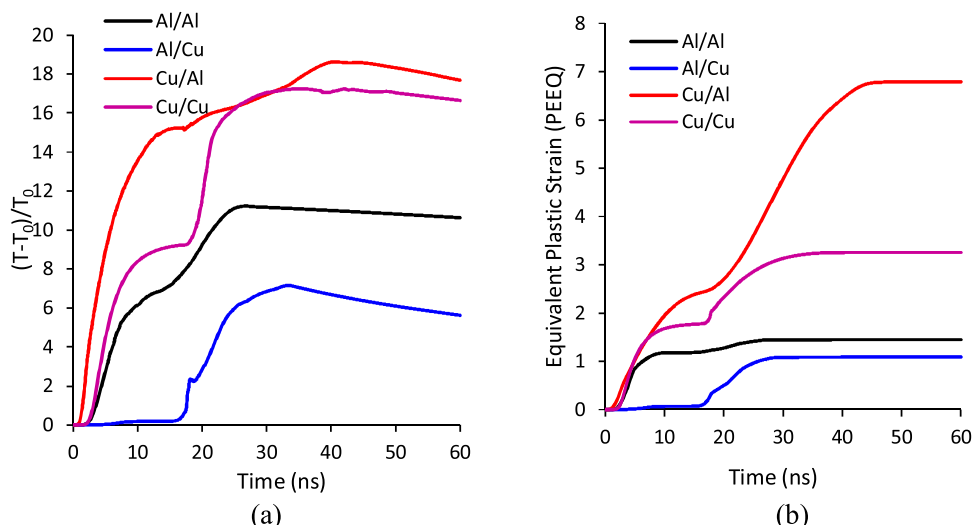


Fig. 15. The impact time of (a) the temperature (TEMP) (b) the equivalent plastic strain (PEEQ) with different materials combination at 50 ms^{-1} using the Lagrangian Numerical approach.

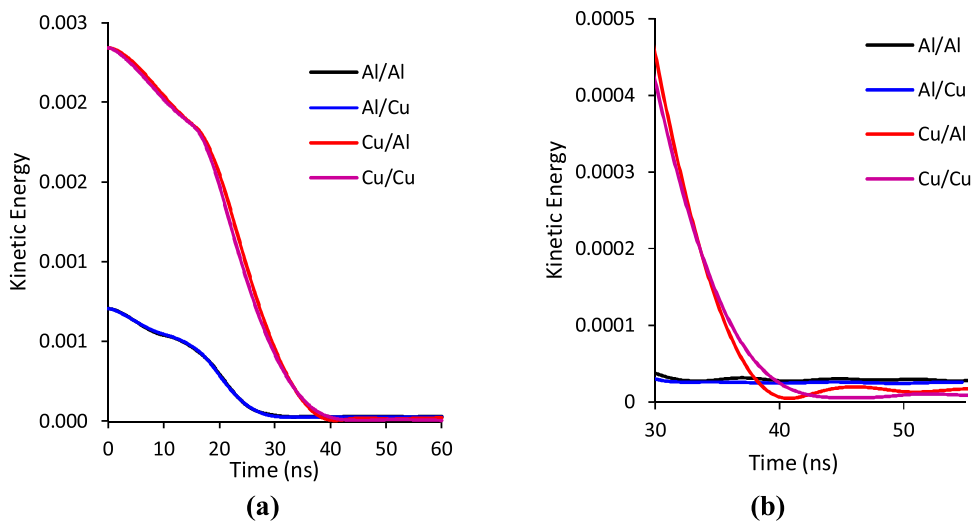


Fig. 16. Normalized kinetic energy for (a) 60 ns; (b) 30 ns–55 ns impact time of different materials combination at 50 ms^{-1} by using the Lagrangian approach.

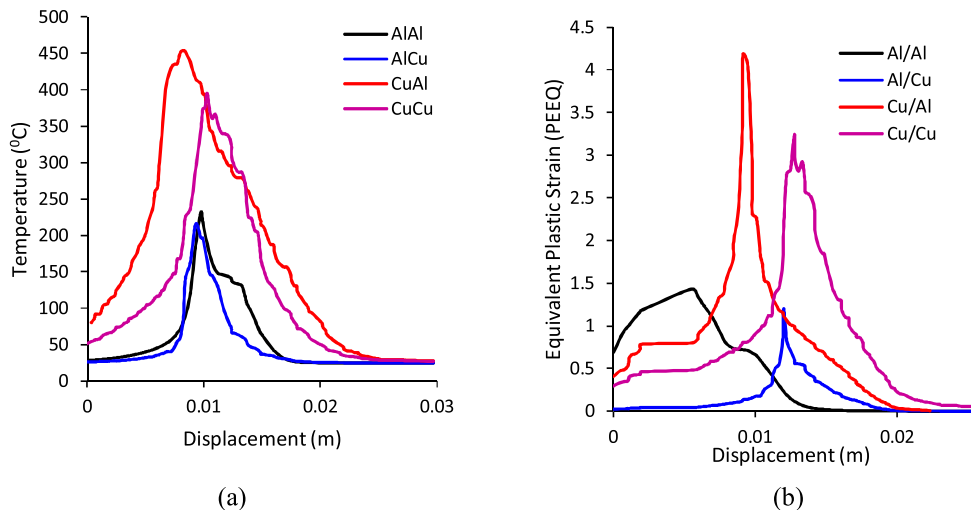


Fig. 17. The Developments of (a) temperature (TEMP) and (b) equivalent plastic strain (PEEQ) along the radial direction of different materials combination at 500 ms^{-1} using the Lagrangian Numerical approach.

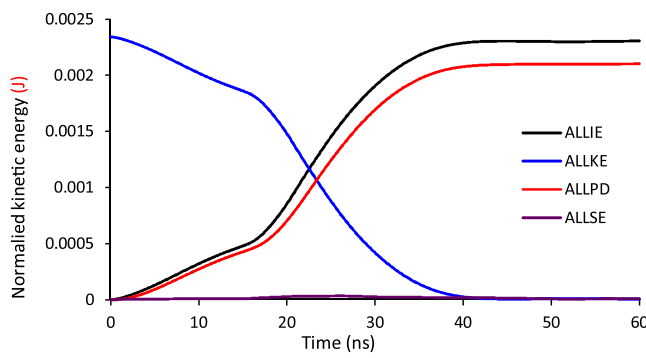


Fig. 18. Normalized kinetic energy of Cu/Cu at a time history of 60 ns at 50 ms^{-1} using the Lagrangian Numerical approach.

In subsequent research, attention will be given to how process parameters affect the quality of the coats rather than the geometry of the particle, impact velocity, temperature and material combination for a given combination of particle/substrate.

4. Conclusion

In the present study, the effects of various processing parameters such as impact velocity, substrate preheating temperature, combinations of different materials and coefficients of friction were used to describe the impact behaviour of ductile materials such as copper and aluminium after deposition. The particle and substrate deformation process occur at supersonic velocity. Therefore, the simulation of material behaviour during impact at high-strain rates and under a large strain must first be addressed. A Lagrangian approach was used to assess the parametric effects on the deposition process of the cold spray model.

At 500 ms^{-1} impact velocity, the impact of four $10 \mu\text{m}$ spherical Cu particles on spherical Cu substrate was studied to analyse the impact behaviour of the typical cold-sprayed process at room temperature. In general, as the impact velocity increases, the initial kinetic energy increases and results in a significant increase in the substrate temperature and plastic strains.

The substrate pre-heating temperature greatly influences the equivalent plastic strain (PEEQ) and the temperature (TEMP) therefore rises within the substrate. Increasing the substrate preheating temperature also increases the maximum temperature which is held below the copper melting point. Therefore, particle and substrate metal

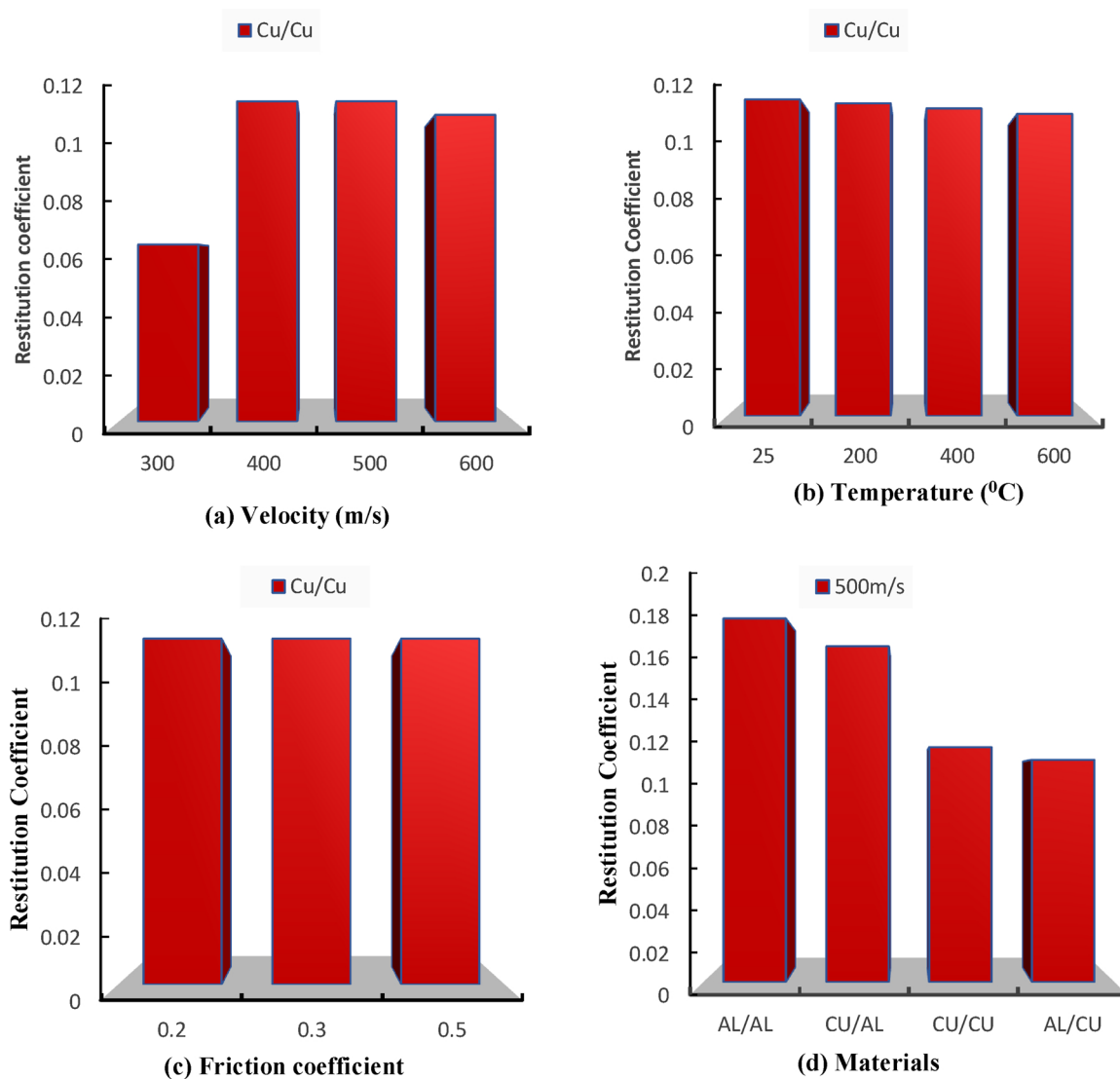


Fig. 19. Restitution coefficients for various process parameters.

Table 3

Schematic illustration of parametric effects on Temperature (TEMP) and equivalent plastic strain (PEEQ).

Variables	ΔTEMP	PEEQ
Velocity	↑↑	↑↑
Pre-heating Temperature	↑	↑↑
Friction	→	↑

cohesion at the interfacial zone occurs without melting, this means that bonding occurs when 60 % of copper melting temperature is attained this is called the bonding temperature. The effect of the coefficient of friction at a distance below the substrate surface on the increase of local temperature is very little, and the PEEQ slightly increases as the friction coefficient increases. This paper reports four different combinations of materials namely: Copper/Copper, Copper/Aluminium, Aluminium/Copper and Aluminium/Aluminium. The influence of particle material is greater than the material of the substrate on the deformation and the deposition process. The Cu particle has initial kinetic energy that is higher because of its higher material density, and this results in higher contact time and larger contact area, and therefore, better particle and

substrate bonding. Cold-spray coating for all the combinations of materials considered in this study is possible provided that the spray is done experimentally with optimised parameters. A lower restitution coefficient was obtained when different materials of varying properties were combined compared to the combination of the same material.

Declaration of Competing Interest

The authors declare that they have no known competing financial interests or personal relationships that could have appeared to influence the work reported in this paper.

Acknowledgement

The authors would like to acknowledge the financial support from University Research Committee (URC) of University of Johannesburg and National Research Foundation (NRF) of South Africa.

References

- [1] R. Ghelichi, M. Guagliano, Coating by the cold spray process: a state of the art, *Frat Ed Integrà Strutt Ed Integrà Strutt* 3 (2009) 30–44, <https://doi.org/10.3221/igf-esis.08.03>.
- [2] W.J. Marple, *The Cold Gas-Dynamic Spray and Characterization of Microcrystalline*

- and Nanocrystalline Copper Alloys, United States Naval Academy, Naval Postgraduate School, 2012.
- [3] J.R. Davis, Handbook of Thermal Spray Technology, ASM International ASM International, Materials Park, OH, USA, 2004.
- [4] F.J. Hermanek, Thermal Spray Terminology and Company Origins, 1st editio, ASM International, Materials Park, OH, USA, 2001.
- [5] E. Irissou, J.-G. Legoux, A.N. Ryabinin, B. Jodoin, C. Moreau, Review on cold spray process and technology: part I - Intellectual property, *J. Therm. Spray Technol.* (2008) 17, <https://doi.org/10.1007/s11666-008-9203-3>.
- [6] R.N. Raoelison, Y. Xie, T. Sapanathan, M.P. Planche, R. Kromer, S. Costil, et al., Cold gas dynamic spray technology: a comprehensive review of processing conditions for various technological developments till to date, *Addit. Manuf.* 19 (2018) 134–159, <https://doi.org/10.1016/j.addma.2017.07.001>.
- [7] H. Singh, T.S. Sidhu, S.B.S. Kalsi, Cold spray technology: future of coating deposition processes, *Frat. Ed. Integrita Strutt* 22 (2012) 69–84, <https://doi.org/10.3221/IGF-ESIS.22.08>.
- [8] D.K. Christoulis, M. Jeandin, E. Irissou, J. Legoux, W. Knapp, Laser-Assisted Cold Spray (LACS) Dimitris, (2012), <https://doi.org/10.5772/36104>.
- [9] A. Moridi, S.M. Hassani-Gangaraj, M. Guagliano, M. Dao, Cold spray coating: review of material systems and future perspectives, *Surf. Eng.* 30 (2014) 369–395, <https://doi.org/10.1179/1743294414y.0000000270>.
- [10] T. Marrocco, D.G. McCartney, P.H. Shipway, A.J. Sturgeon, Production of titanium deposits by cold-gas dynamic spray: numerical modeling and experimental characterization, *J. Therm. Spray Technol.* 15 (2006) 263–272, <https://doi.org/10.1361/105996306X108219>.
- [11] D. MacDonald, R. Fernández, F. Delloro, B. Jodoin, Cold spraying of armstrong process titanium powder for additive manufacturing, *J. Therm. Spray Technol.* 26 (2017) 598–609, <https://doi.org/10.1007/s11666-016-0489-2>.
- [12] T.H. Van Steenkiste, J.R. Smith, R.E. Teets, Aluminum coatings via kinetic spray with relatively large powder particles, *Surf. Coat. Technol.* 154 (2002) 237–252, [https://doi.org/10.1016/S0257-8972\(02\)00018-X](https://doi.org/10.1016/S0257-8972(02)00018-X).
- [13] M. Grujicic, C.L. Zhao, C. Tong, W.S. DeRosset, D. Helfritch, Analysis of the impact velocity of powder particles in the cold-gas dynamic-spray process, *Mater. Sci. Eng. A* 368 (2004) 222–230, <https://doi.org/10.1016/j.msea.2003.10.312>.
- [14] H. Assadi, F. Gartner, T. Stoltenhoff HK, Bonding mechanism in cold gas spraying, *Acta Mater. Inc.* 51 (2003) 4379–4394.
- [15] A. Viscusi, A. Astarita, L. Carrino, G. D'Avino, C. de Nicola, P.L. Maffettone, et al., Experimental study and numerical investigation of the phenomena occurring during long duration cold spray deposition, *Int. Rev. Model. Simul.* 11 (2018) 84–92, <https://doi.org/10.15866/fremos.v11i2.13619>.
- [16] W.Y. Li, D.D. Zhang, C.J. Huang, S. Yin, M. Yu, F.F. Wang, et al., Modelling of impact behaviour of cold spray particles: review, *Surf. Eng.* (2014), <https://doi.org/10.1179/1743294414Y.0000000268>.
- [17] T. Hussain, Cold spraying of titanium: a review of bonding mechanisms, microstructure and properties, *Key Eng. Mater.* Online 533 (2013) 53–90, <https://doi.org/10.4028/www.scientific.net/KEM.533.53>.
- [18] F. Meng, D. Hu, Y. Gao, S. Yue, J. Song, Cold spray bonding mechanisms and deposition efficiency prediction for particle/substrate with distinct deformability, *Jmadae* 109 (2016) 503–510, <https://doi.org/10.1016/j.matdes.2016.07.103>.
- [19] L. Zhu, T.C. Jen, H.S. Chen, Particle bonding mechanism in cold gas dynamic spray: a three-dimensional approach, *J. Therm. Spray Technol.* 26 (2017) 1859–1873, <https://doi.org/10.1007/s11666-017-0652-4>.
- [20] T. Hussain, D.G. McCartney, P.H. Shipway, Bonding between aluminium and copper in cold spraying: story of asymmetry, *Mater. Sci. Technol.* 28 (2012) 1371–1378, <https://doi.org/10.1179/1743284712Y.0000000051>.
- [21] M. Grujicic, C. Zhao, W. DeRosset, D. Helfritch, Adiabatic shear instability based mechanism for particles/substrate bonding in the cold-gas dynamic-spray process, *Mater. Des.* 25 (2004) 681–688, <https://doi.org/10.1016/j.matdes.2004.03.008>.
- [22] R.C. Dykhuizen, M.F. Smith, D.L. Gilmore, R.A. Neiser, X. Jiang, S. Sampath, Impact of high velocity cold spray particles, *J. Therm. Spray Technol.* 8 (1999) 559–564, <https://doi.org/10.1361/105996399770350250>.
- [23] A. Malachowska, Analysis of the cold gas spraying process and determination of selected properties of metallic coatings on polymers, *Materials, Université de Limoges, 2016 English. fnfNT: 2016LIMO0012f*.
- [24] T. Klassen, H. Assadi, H. Kreye, Cold spraying e A materials perspective, *Acta Mater.* 116 (2016) 382–407, <https://doi.org/10.1016/j.actamat.2016.06.034>.
- [25] H. Assadi, F. Gartner, T. Stoltenhoff, Bonding mechanism in cold gas spraying, *Acta Mater. Inc.* 6454 (2003) 4379–4394, [https://doi.org/10.1016/S1359-6454\(03\)00274-X](https://doi.org/10.1016/S1359-6454(03)00274-X).
- [26] A. Viscusi, Numerical investigations on the rebound phenomena and the bonding mechanisms in cold spray processes, *AIP Conf. Proc.* American Institute of Physics Inc., 2018, <https://doi.org/10.1063/1.5034957> vol. 1960.
- [27] W. Li, C. Zhang, C.L.H. Li, Modeling aspects of high velocity impact of particles in cold spraying by explicit finite element analysis, *J. Therm. Spray Technol.* 18 (2009) 921–933, <https://doi.org/10.1007/s11666-009-9325-2>.
- [28] W.Y. Li, W. Gao, Some aspects on 3D numerical modeling of high velocity impact of particles in cold spraying by explicit finite element analysis, *Appl. Surf. Sci.* 18 (2009) 7878–7892, <https://doi.org/10.1016/j.apsusc.2009.04.135>.
- [29] Y. Shuo, X. Wang, W.X.B. Li, Numerical investigation on effects of interactions between particles on coating formation in cold spraying, *J. Therm. Spray Technol.* 18 (2009) 686–698, <https://doi.org/10.1007/s11666-009-9390-6>.
- [30] S. Yin, X.-F. Wang, W.Y. Li, H.-E. Jie, Effect of substrate hardness on the deformation behavior of subsequently incident particles in cold spraying, *Appl. Surf. Sci.* 257 (2011) 7560–7565, <https://doi.org/10.1016/j.apsusc.2011.03.126>.
- [31] K. Moonga, T.C. Jen, Numerical Analysis of the Cold Gas Dynamic Spray Surface Coating Process Numerical Analysis of the Cold Gas Dynamic Spray Surface Coating Process, (2017), pp. 1–6, <https://doi.org/10.2991/icmme-17.2017.13>.
- [32] T.C. Jen, et al., Numerical investigations on cold gas dynamic spray process with nano- and microsize particles, *Int. J. Heat Mass Transf.* 48 (2005) 4384–4396, <https://doi.org/10.1016/j.ijheatmasstransfer.2005.05.008>.
- [33] K. Moonga, T.C. Jen, Numerical analysis of the cold gas dynamic spray surface coating process, *Adv. Eng. Res.* 102 (2017) 75–79, <https://doi.org/10.2991/icmme-17.2017.13>.
- [34] M. Yu, W. Li, F.F. Wang, H.L. Liao, Finite element simulation of impacting behavior of particles in cold spraying by Eulerian approach, *J. Therm. Spray Technol.* 21 (2012) 744–752, <https://doi.org/10.1007/s11666-011-9717-y>.
- [35] B. Yildirim, S. Muffu, A. Gouldstone, Modeling of high velocity impact of spherical particles, *Wear* 270 (2011) 703–713.
- [36] R. Ghelichi, S. Bagherifard, M.V.M. Guagliano, Numerical simulation of cold spray coating, *Surf. Coat. Technol.* 205 (2011) 5294–5301.
- [37] G. Bae, Y. Xiong, S. Kumar, K. Kang, C. Lee, General aspects of interface bonding in kinetic sprayed coatings, *Acta Mater.* 56 (2008) 4858–4868, <https://doi.org/10.1016/j.actamat.2008.06.003>.
- [38] A. Manap, K. Ogawa, T. Okabe, Numerical analysis of interfacial bonding of Al-Si particle and mild steel substrate by cold spray technique using the SPH method, *J. Solid Mech. Mater. Eng.* 6 (2012) 241–250, <https://doi.org/10.1299/jmmpp.6.241>.
- [39] A. Manap, T.O.K. Okabe, Computer simulation of cold sprayed deposition using smoothed particle hydrodynamics, *Procedia Eng.* 10 (2011) 1145–1150, <https://doi.org/10.1016/j.proeng.2011.04.190>.
- [40] A. Manap, T. Okabe, K. Ogawa, S. Mahalingam, H. Abdullah, Experimental and smoothed particle hydrodynamics analysis of interfacial bonding between aluminum powder particles and aluminum substrate by cold spray technique, *Int. J. Adv. Manuf. Technol.* 103 (2019) 4519–4527, <https://doi.org/10.1007/s00170-019-03846-4>.
- [41] W. Li, S. Yin, X. Wang, Numerical investigations of the effect of oblique impact on particle deformation in cold spraying by the SPH method, *Appl. Surf. Sci.* 256 (2010) 3725–3734, <https://doi.org/10.1016/j.apsusc.2010.01.014>.
- [42] S. Yin, X. Wang, B. Xu, W. Li, Examination on the calculation method for modeling the multi-particle impact process in cold spraying, *J. Therm. Spray Technol.* 19 (2010) 1032–1041, <https://doi.org/10.1007/s11666-010-9489-9>.
- [43] I. Smoijer, D. Ivancic, Bird strike damage analysis in aircraft structures using Abaqus/Explicit and coupled Eulerian Lagrangian approach, *Compos. Sci. Technol.* 71 (2011) 489–498, <https://doi.org/10.1016/j.compscitech.2010.12.024>.
- [44] G. Qiu, S. Henke, J. Grabe, Application of a Coupled Eulerian-Lagrangian approach on geomechanical problems involving large deformations, *Comput. Geotech.* 88 (2011) 30–39, <https://doi.org/10.1016/j.compgeo.2010.09.002>.
- [45] J.M. Mbuyamba, Calculation and Design of Supersonic Nozzles for Cold Gas Dynamic Spraying Using MATLAB and ANSYS Fluent, University of the Witwatersrand, Johannesburg, 2013.
- [46] M. Karimi, A. Fartaj, G. Rankin, D. Vanderz wet, W. Birtch, J. Villafuerte, Numerical simulation of the cold gas dynamic spray process, *Proc. Int. Therm. Spray Conf.* 15 (2006) 518–523, <https://doi.org/10.1361/105996306X146866>.
- [47] W. Li, H. Liao, G. Douchy, C. Coddet, Materials & Design Optimal design of a cold spray nozzle by numerical analysis of particle velocity and experimental validation with 316L stainless steel powder, *Mater. Des.* 28 (2007) 2129–2137, <https://doi.org/10.1016/j.matdes.2006.05.016>.
- [48] S. Garmeh, M. Jadidi, A. Dolatabadi, Three-dimensional modeling of cold spray for additive manufacturing, *J. Therm. Spray Technol.* (2019), <https://doi.org/10.1007/s11666-019-00928-3>.
- [49] Abaqus Analysis User's Manual, ABAQUS 6.14 HTML Documentation, Dassault Systemes, (2014).
- [50] A. Manap, K. Ogawa, T. Okabe, Numerical analysis of interfacial bonding of aluminum powder particle and aluminum substrate by cold spray technique using the SPH method, *Proc. JSME/ASME 2011 ICMP2011*, Corvallis, Oregon, USA, Orvallis, Oregon, USA, 2011.
- [51] X. Jing, D. Nélias, H.O. Walter-Leberre, Y. Ichikawa, Simulation of the cold spray deposition process for aluminium and copper using lagrangian, ALE and CEL methods, *J. Tribol.* (2015) 137, <https://doi.org/10.1115/1.4032057>.
- [52] P.C. King, S.H. Zahiri, M. Jahedi, Microstructural refinement within a cold-sprayed copper particle, *Metall. Mater. Trans. A* 40 (2009) 2115–2123, <https://doi.org/10.1007/s11661-009-9882-5>.
- [53] W.-Y. Li, S. Yin, X.-F. Wang, Numerical investigations of the effect of oblique impact on particle deformation in cold spraying by the SPH method, *Appl. Surf. Sci.* 256 (2010) 3725–3734, <https://doi.org/10.1016/j.apsusc.2010.01.014>.
- [54] H. Assadi, F. Gärtner, T. Stoltenhoff, H. Kreye, Bonding mechanism in cold gas spraying, *Acta Mater.* 51 (2003) 4379–4394, [https://doi.org/10.1016/S1359-6454\(03\)00274-X](https://doi.org/10.1016/S1359-6454(03)00274-X).
- [55] J. Vlcek, L. Gimeno, H. Huber, E. Lugscheider, A systematic approach to material eligibility for the cold-spray process, *J. Therm. Spray Technol.* 14 (2005) 125–133, <https://doi.org/10.1361/10599630522738>.
- [56] C.-Y. Wu, Finite Element Analysis of Particle Impact Problems. PhD Thesis, Aston University, Birmingham, UK, 2001.
- [57] S.W.H. Faik, Modeling of impact dynamics: a literature survey, *Int. ADAMS User Conf.* Toronto Canada (2000).
- [58] S.V. Klinkov, V. Fedorovich Kosarev, M. Rein, Cold spray deposition: significance of particle impact phenomena, *Aerosp. Sci. Technol.* 9 (2005) 582–591, <https://doi.org/10.1016/j.ast.2005.03.005>.
- [59] K.H. Moonga, T.C. Jen, Film surface characterization in cold spray using advanced numerical modeling and simulation techniques, *Int. J. Mech. Eng. Robot. Res.* 7 (2018) 66–71, <https://doi.org/10.18178/jimerr.7.1.66-71>.
- [60] A. Manap, O. Nooririnah, H. Misran, T. Okabe, K. Ogawa, Experimental and SPH study of cold spray impact between similar and dissimilar metals, *Surf. Eng.* 30 (2014) 335–341, <https://doi.org/10.1179/1743294413Y.0000000237>.
- [61] J. Lee, S. Shin, H. Kim, C. Lee, Effect of gas temperature on critical velocity and deposition characteristics in kinetic spraying, *Appl. Surf. Sci.* 253 (2007) 3512–3520, <https://doi.org/10.1016/j.apsusc.2006.07.061>.
- [62] S.T. Oyinbo, T.-C. Jen, A comparative review on cold gas dynamic spraying processes and technologies, *Manuf. Rev.* 6 (25) (2019) 1–20, <https://doi.org/10.1051/mfreview/2019023>.